Nanoscale

COMMUNICATION

View Article Online
View Journal | View Issue

Published on 14 December 2015. Downloaded by Michigan State University on 21/01/2016 20:19:10.

Cite this: *Nanoscale*, 2016, **8**, 1327

Received 14th October 2015,
Accepted 12th December 2015

DOI: 10.1039/c5nr07122d

www.rsc.org/nanoscale

# Ultrahigh mobility in polyolefin-supported graphene†

Ya-Ping Hsieh,*[a] Chin-Lun Kuo[a] and Mario Hofmann[b]

**A high carrier mobility is an important parameter for graphene-based electronics. While the recent reports have shown impressive results for individual micro-scale devices, scalable production of high mobility graphene has been challenging. We here show that centimeter-scale graphene devices with room temperature carrier mobilities in excess of 10 000 $cm^2\ V^{-1}\ s^{-1}$ can be achieved on polyolefinic substrates. Measurements on Parafilm-supported graphene devices show, on average, a fivefold-enhancement in mobility over traditional devices. We find that a decreased charged-impurity scattering is the origin of this behavior. Spectroscopic characterization reveals oxygen-containing polymer residue as the main source of such charged impurities. A comparison of different polyolefins highlights the positive impact of oxygen-free polymers as support materials for high mobility graphene devices. Finally, moldable and wearable graphene devices for biosensors were shown to be enabled by polyolefinic substrates.**

## Introduction

Graphene-based electronics that exploit the unique characteristics of this two-dimensional carbon allotrope are expected to enable novel applications such as high speed device amplifiers[1] or exotic device concepts.[2–4] Both the scientific research and commercialization of such devices require the scalable synthesis of graphene with consistent and high mobility.[5] Macroscopic devices and wafer-scale arrays of devices, however, are yet to show uniform mobilities in excess of $\mu = 10^4\ cm^2\ V^{-1}\ s^{-1}$.[6]

The origin of this low achievable carrier mobility is the occurrence of charge puddles brought about by inhomogeneous charge transfer between graphene and commonly used $Si/SiO_2$ substrates.[7] Significant research effort has been invested in finding alternative substrates that can limit the impact of those charged scatterers. Graphene devices on boron-nitride single crystals,[8] for example, have yielded up to 10 fold improvement in the carrier mobility but the requirement for high quality BN crystals makes this approach not scalable.

Polymeric supports could provide an alternative route for enhancing the graphene mobility since their chemical structure could be tuned to minimize interaction with graphene. Martins *et al.*[9] investigated the effect of various polymeric supports on the graphene quality but found no enhancement of the graphene performance.

We here demonstrate that polyolefinic support films can overcome both issues and significantly enhance the large-scale mobility of graphene devices. We found that polyolefins will induce less charged impurities than traditional support materials which results in significantly improved mobilities. Spectroscopic analysis reveals that the absence of oxygen-containing functional groups is a requirement for high mobility graphene. Finally, polyolefinic layers can be employed as mechanically stable and conformable substrates for wearable sensors and flexible devices.

## Experimental

Graphene was grown by CVD on electropolished copper foil (99.8%, Alfa-Aesar, no. 13382) at 1000 °C for 30 minutes with flow ratios of $H_2 : CH_4 = 20 : 1$ at a total pressure of 9 torr following previous reports.[10] Poly(methyl methacrylate, Microchem A9) (PMMA)-supported devices were produced by posi-

[a]*Graduate of Institute of Opto-Mechatronics, National Chung Cheng University, 168, University Rd., Min-Hsiung, Chia-Yi, 62102, Taiwan. E-mail: yphsieh@ccu.edu.tw*
[b]*Department of Material Science and Engineering, National Cheng Kung University, Tainan, 62102, Taiwan*

†Electronic supplementary information (ESI) available: Optical micrographs of oxidation tests; comparison of different characterization methods; extended characterization of graphene grown using various cap materials; large scale uniformity of graphene characterization of OM after etching. See DOI: 10.1039/c5nr07122d

Published on 14 December 2015. Downloaded by Michigan State University on 21/01/2016 20:19:10.

tioning the floating PMMA/graphene structure from a water bath onto a $SiO_2$ wafer with buried electrodes. Polyolefin-supported devices were produced by placing the support on top of graphene and heating the structure to 100 °C while applying moderate pressures to ensure good contact. After cooling, the polyolefin/graphene/copper stack was immersed in $FeCl_3$ etchant to remove the copper. The polyolefin-supported graphene was then washed in deionized water and dried under a stream of dry nitrogen. Electrical contact with the graphene devices was made using Ag paint (Ted Pella, 16034). The sheet resistance and Hall-effect mobility were measured using a 4-point probe in van-der-Pauw geometry with a sample size of $1 \times 1$ cm$^2$. Raman measurements were performed in a home-built micro-Raman system using a 532 nm laser excitation source.

## Results and discussion

Commercially available Parafilm M® (Bemis Company, Inc.) was used as a support material for initial experiments. The material is widely used in laboratories and consists of short-chain polyolefins.[11] Hall-effect measurements of graphene on Parafilm reveal unusually higher carrier mobilities compared to graphene on PMMA (Fig. 1(a)). While CVD-grown graphene on the PMMA support exhibits average mobilities of $\mu$ = 929 cm$^2$ V$^{-1}$ s$^{-1}$, similar to the reported values for graphene on the $SiO_2$ support,[12] graphene on the Parafilm substrate shows average mobilities of $\mu$ = 5595 cm$^2$ V$^{-1}$ s$^{-1}$ with 10% of the devices exceeding mobilities of $\mu$ = 10 000 cm$^2$ V$^{-1}$ s$^{-1}$. These values are even more impressive when considering that they were obtained from macroscopic ($1 \times 1$ cm$^2$) films which are expected to have much lower mobility compared to micrometer scale devices due to the occurrence of grain boundaries and handling-induced damage.

We attempt to elucidate the observed enhancement in mobility by carrier concentration measurements. Fig. 1(b) shows the extracted values for mobility and carrier concentration for devices on the Parafilm-support and on the PMMA-support. The observed inverse proportionality indicates that the mobility is high for Parafilm samples which show low carrier concentrations and low for PMMA samples which exhibit high carrier concentrations.

Such behavior is in agreement with predictions for transport in the presence of charged impurities: increasing impurity concentrations enhance the carrier density through charge transfer but deteriorate the carrier mobility by electrostatic interactions. Previous reports found that these two effects have inverse dependences on the impurity concentration[13] and thus result in the observed trend. We can therefore conclude that the decrease in charged impurities is causing the high mobility of graphene on Parafilm compared to other substrates. Interestingly, the reduction in dopants seems to not affect their sample-to-sample variation and similar variabilities of $\mu = 10^{12}$ cm$^{-2}$ were observed and correlated with water adsorption on graphene (ESI Fig. S1†). While the impact of environmental contaminants is relatively small for graphene on PMMA the low intrinsic scatterer concentration of graphene on Parafilm is overwhelmed by those adsorbates which explain the large scattering in the values of carrier mobility. Future studies have to establish the limits of reduction in the device variability and the maximum achievable carrier mobilities under controlled-environmental conditions.

The performance of Parafilm-supported graphene is not only superior to PMMA-supported graphene but also to graphene that was transferred onto $SiO_2$/Si substrates which exhibited mobilities of $\mu$ = 1094 cm$^2$ V$^{-1}$ s$^{-1}$. We now attempt to identify the origin of this behavior.

To elucidate whether the interaction with $SiO_2$ deteriorates the quality of graphene, we carried out graphene transfer using Parafilm and PMMA. For this purpose, Parafilm was removed by immersion in chloroform while transfer using PMMA was conducted following established procedures.[14] Fourier-transform infrared (FTIR) spectroscopy was conducted before and after Parafilm removal (Fig. 2(a)). The absence of the characteristic paraffin C–H stretching modes[15] at 2956 cm$^{-1}$, 2919 cm$^{-1}$ and 2850 cm$^{-1}$ in the latter spectrum indicates the removal of Parafilm. This result is supported by Raman spectroscopy (Fig. 2(b)). Here, the characteristic $CH_2$ deformations[16] around 1441 cm$^{-1}$ and 2881 cm$^{-1}$ are absent after the removal of Parafilm. Finally, atomic force microscopy demonstrates the low amounts of residue introduced after

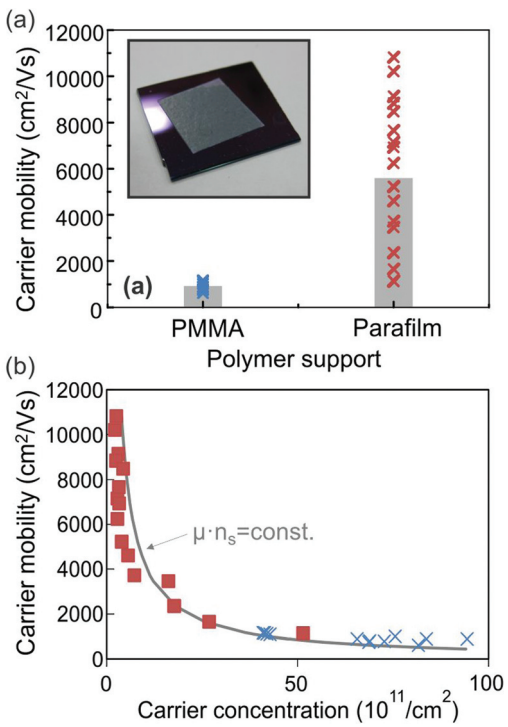


**Fig. 1** (a) Comparison of carrier mobility of graphene supported by PMMA and Parafilm, (b) relationship between carrier mobility and concentration for both support materials.


This journal is © The Royal Society of Chemistry 2016

Published on 14 December 2015. Downloaded by Michigan State University on 21/01/2016 20:19:10.

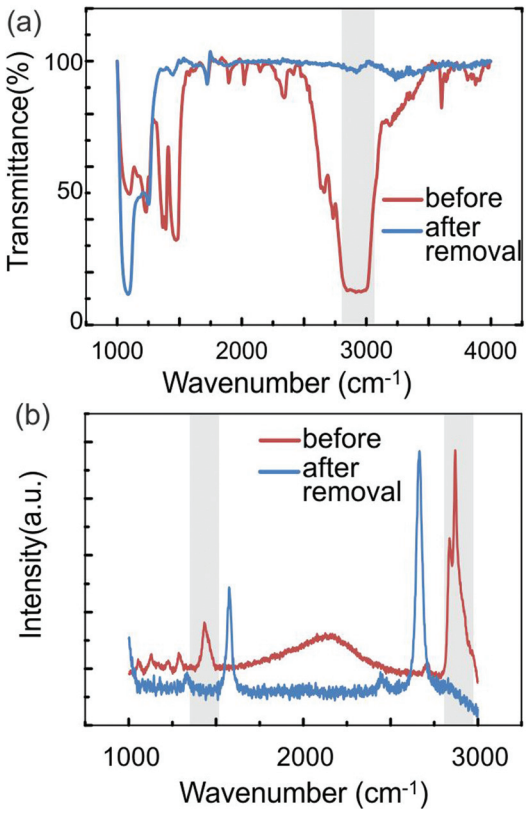


Fig. 2 (a) FTIR spectra before and after Parafilm removal indicating suppression of C–H vibrations at 3000 $cm^{-1}$, (b) Raman spectra before and after Parafilm removal with indication of suppressed Parafilm Raman peaks.

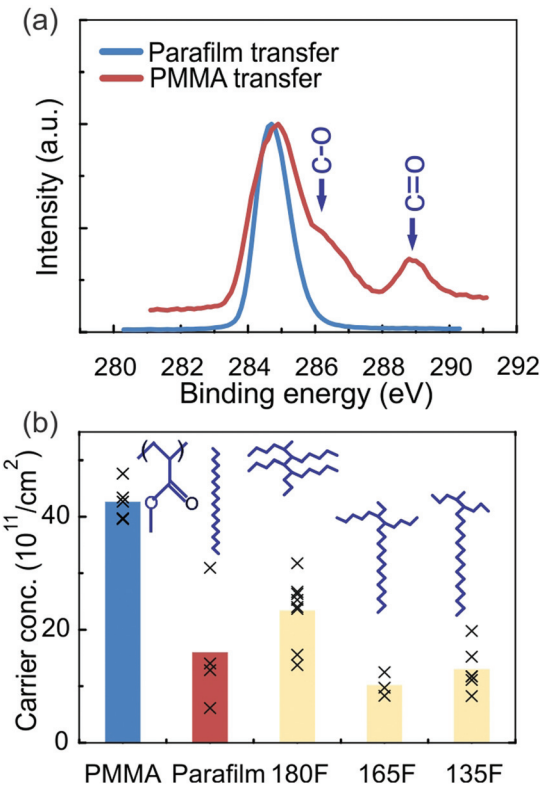


Fig. 3 (a) XPS spectra of graphene samples after PMMA and Parafilm transfer, (b) comparison of carrier concentration for various paraffin waxes indicating a consistently smaller doping than PMMA samples.

both transfer processes which could be further decreased in the future by optimized transfer protocols (ESI Fig. S5†).

With the completeness of Parafilm removal established, we turn to explaining the observed difference in charged impurity concentration.

Electrical measurements after removal of the polymers show a decrease in carrier concentration for graphene after PMMA removal by 35%. Conversely, the removal of Parafilm increases the carrier density of graphene by 32%. The different trends are also reflected in the carrier mobility with PMMA-removal increasing the mobility while Parafilm-removal decreasing the mobility.

To elucidate the origin of this behavior, graphene after PMMA and Parafilm removal was investigated by X-ray photoelectron spectroscopy (XPS). The carbon 1s peak of the Parafilm-removed graphene is significantly sharper than the PMMA-removed graphene (Fig. 3(a)). The deconvolution of the C 1s peak reveals a 9-fold decrease in C–O bond concentration relative to the C–C bond concentration between graphene after PMMA and Parafilm removal (ESI Fig. S1†). Furthermore, the C═O to C–C bond ratio decreased from 17% for the PMMA-removed graphene to below the detection threshold for the Parafilm-removed graphene.

The C–O bonds could originate from functional groups in graphene[17] or from the oxygen-containing polymer residue.[18] Since XPS is not able to detect the difference between these two oxygen sources, we turn to Raman spectroscopy. Due to their difference in bonding geometry, functional groups in direct contact with graphene will give rise to a Raman D-band peak around 1350 $cm^{-1}$.[19] We find that graphene after the PMMA removal exhibits comparable D-band intensities to graphene after the Parafilm removal (ESI Fig. S2†). Consequently, the C–O bonds are thought to originate from the polymer residue. This finding can also explain the here reported changes in graphene's carrier concentration after the polymer-removal. While the removal of PMMA causes a decrease in oxygen-containing residue and carrier concentration, Parafilm does not contain oxygen and its removal exposes graphene to the environment, thus increasing the concentration of scatterers.

Based on these findings, we identify the defining property that makes Parafilm a superior support as the absence of oxygen-containing groups in its structure. Based on this hypothesis, other polymers which share this characteristic should result in graphene with lower impurity concentrations than the PMMA-transferred graphene.

We investigate graphene transfer using a multitude of different polyolefins to prove this point. Paraffin waxes are a

Published on 14 December 2015. Downloaded by Michigan State University on 21/01/2016 20:19:10.

by-product of oil refining that contain mixtures of short-chained alkenes and are characterized by their melting points. Despite their low purity and significant differences in structure, transfer with the investigated paraffin waxes causes 50% to 75% lower carrier concentration than the PMMA-transferred graphene (Fig. 3b). The presented results suggest the use of polyolefins for high quality transfer for future graphene applications such as high speed transistors (ESI Fig. S3†).

In addition to the enhanced performance, polyolefin-supported graphene devices exhibit other attractive features. Due to its flexibility, mechanical strength, and plastic deformability, the substrate lends itself to the production of wearable and moldable graphene devices.

To illustrate this point, we fabricated a simple and large-scale graphene device on Parafilm. A flexible connector was employed to make contact between a source meter and two silver electrodes at the corners of the device (inset of Fig. 4(a)). We measured the resistance of the Parafilm-supported graphene device before and after molding it onto skin (Fig. 4(a)). The current–voltage diagram in Fig. 4(a) shows that the attachment procedure has not damaged the graphene device. Furthermore, a change in conductivity indicates an interaction of the graphene device with the skin. Further experiments will have to elucidate the sensing mechanism.[20] Fig. 4(b) shows the current change upon repeated contact of the device with the skin and a fast and repeatable conductance change is observable.

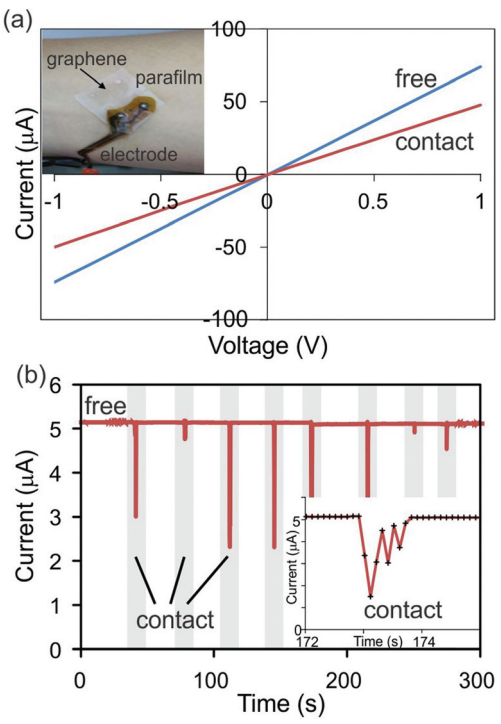


Fig. 4 (a) IV sweeps before and after attachment of the device on the skin (inset photograph of the Parafilm supported graphene device molded onto the skin), (b) current change upon repeated contact/removal procedures (voltage = 0.1 V).

The presented low impurity concentration and mechanical stability in combination with the established biocompatibility of polyolefinic support layers[21] make our approach ideally suited for graphene-based wearable and even implantable sensors.[22]

## Conclusions

In conclusion, we have demonstrated the potential of using polyolefins for graphene transfer. A significant reduction in impurity concentration leads to enhanced carrier transport and unprecedentedly high large-scale film mobilities in excess of $\mu = 10\,000$ cm$^2$ V$^{-1}$ s$^{-1}$. Spectroscopic characterization reveals that the absence of oxygen-containing residues is the origin of this effect. We therefore recommend the use of polyolefins as a promising approach for supporting or transferring high-speed graphene devices.

## Acknowledgements

Y. P. Hsieh and M. Hofmann acknowledge financial support from Applied Materials, Inc., the Ministry of Science and Technology, and the Industrial Technology Research Institute of Taiwan.

## References

1 Y.-M. Lin, K. A. Jenkins, A. Valdes-Garcia, J. P. Small, D. B. Farmer and P. Avouris, *Nano Lett.*, 2009, **9**, 422–426.
2 L. F. Register, X. Mou, D. Reddy, W. Jung, I. Sodemann, D. Pesin, A. Hassibi, A. H. MacDonald and S. K. Banerjee, *ECS Trans.*, 2012, **45**, 3–14.
3 D. Gunlycke and C. T. White, *Phys. Rev. Lett.*, 2011, 106.
4 W. Han, R. K. Kawakami, M. Gmitra and J. Fabian, *Nat. Nanotechnol.*, 2014, **9**, 794–807.
5 A. Zurutuza and C. Marinelli, *Nat. Nanotechnol.*, 2014, **9**, 730–734.
6 S. Rahimi, L. Tao, S. F. Chowdhury, S. Park, A. Jouvray, S. Buttress, N. Rupesinghe, K. Teo and D. Akinwande, *ACS Nano*, 2014, **8**, 10471–10479.
7 Y. Zhang, V. W. Brar, C. Girit, A. Zettl and M. F. Crommie, *Nat. Phys.*, 2009, **5**, 722–726.
8 W. Gannett, W. Regan, K. Watanabe, T. Taniguchi, M. F. Crommie and A. Zettl, *Appl. Phys. Lett.*, 2011, **98**, 242105.
9 L. G. Martins, Y. Song, T. Zeng, M. S. Dresselhaus, J. Kong and P. T. Araujo, *Proc. Natl. Acad. Sci. U. S. A.*, 2013, **110**, 17762–17767.
10 Y.-P. Hsieh, M. Hofmann, K.-W. Chang, J. G. Jhu, Y.-Y. Li, K. Y. Chen, C. C. Yang, W.-S. Chang and L.-C. Chen, *ACS Nano*, 2014, **8**, 443–448.
11 P. Gaskin, J. MacMillan, R. D. Firn and R. J. Pryce, *Phytochemistry*, 1971, **10**, 1155–1157.

 This journal is © The Royal Society of Chemistry 2016

Published on 14 December 2015. Downloaded by Michigan State University on 21/01/2016 20:19:10.

12 G. Borin Barin, Y. Song, I. de Fátima Gimenez, A. G. Souza Filho, L. S. Barreto and J. Kong, *Carbon*, 2015, **84**, 82–90.
13 J. Yan and M. S. Fuhrer, *Phys. Rev. Lett.*, 2011, **107**, 206601.
14 M. Hofmann, Y. P. Hsieh, A. L. Hsu and J. Kong, *Nanoscale*, 2014, **6**, 289–292.
15 E. Lee, Y.-S. Lee and K.-H. Lim, *Korean J. Chem. Eng.*, 2010, **27**, 518–523.
16 M. A. Puerto and N. M. Balzaretti, *Vib. Spectrosc.*, 2014, **75**, 93–100.
17 L. R. Radovic, A. B. Silva-Tapia and F. Vallejos-Burgos, *Carbon*, 2011, **49**, 4218–4225.
18 Y.-C. Lin, C. Jin, J.-C. Lee, S.-F. Jen, K. Suenaga and P.-W. Chiu, *ACS Nano*, 2011, **5**, 2362–2368.
19 L. G. Cancado, A. Jorio, E. H. Ferreira, F. Stavale, C. A. Achete, R. B. Capaz, M. V. Moutinho, A. Lombardo, T. S. Kulmala and A. C. Ferrari, *Nano Lett.*, 2011, **11**, 3190–3196.
20 Y. Shao, J. Wang, H. Wu, J. Liu, I. A. Aksay and Y. Lin, *Electroanalysis*, 2010, **22**, 1027–1036.
21 S. J. Yoo and Y. Nam, *J. Neurosci. Methods*, 2012, **204**, 28–34.
22 K. Kostarelos and K. S. Novoselov, *Nat. Nanotechnol.*, 2014, **9**, 744–745.